RSC Advances

ROYAL SOCIETY OF CHEMISTRY

www.rsc.org/advances

Journal Name

RSCPublishing

ARTICLE

Spin-dependent electronic transport properties of zigzag Silicon Carbon nanoribbon

Cite this: DOI: 10.1039/xoxxoooooox

Yipeng An*[a], Mengjun Zhang[a], Lipeng Chen[b], Congxin Xia*[a], Tianxing Wang[a], Zhaoming Fu[ac], Zhaoyong Jiao[a], and Guoliang Xu[a]

Received ooth January 2012,
Accepted ooth January 2012

DOI: 10.1039/xoxxoooooox

www.rsc.org/

Spin-dependent electronic transport properties of the zigzag Silicon Carbon nanoribbon (Z-SiCNR) are studied by employing the non-equilibrium Green's function method in the framework of density functional theory. It is found that the Z-SiCNR exhibits a variety of exotic physical properties. While the Z-SiCNR in the metallic FM state presents spin filtering and current-limited effects, it is shown that the abnormal oscillation of spin-polarized currents with spin polarization as high as 100% under certain bias voltage emerges in the half-metallic AFM state. The results demonstrate that tuning the spin state of the zigzag SiC nanoribbon provides a possible avenue to design next generation spin nanodevice with novel functionalities.

Introduction

Spintronic devices have garnered ever increasing attention due to the fact that it is more efficient to carry information through manipulating electron spin rather than the charge.[1] This interest in the studies of spintronics is largely stimulated by a variety of industrial applications, ranging from read-heads in hard disk drives, magnetic random access memory to spin filters.

Through the past decade, graphene and some graphene-like materials, such as BN, SiC nanosheets and nanoribons, have been proposed as the potential candidates for the applications in spintronics.[2-18] Since the first report of the preparation and isolation of single graphene layer in 2004,[2] several prototype devices based on graphene have been fabricated in laboratory.[3-5] The electronic transport properties of various graphene-based devices have also been extensively studied theoretically.[6-8] For the graphene-like materials, BN, also called "white graphene", exhibits superior electronic and transport properties, such as spin filtering, magneto-resistance[9] and negative differential resistance effects[10] apart from its high stability under oxidized environment (stable up to 900 in air[11]). Recently, the successful fabrication of SiC nanotubes[12] as well as the theoretical prediction of the stability of graphene-like SiC monolayers[13,14] have in particular attracted extensive interest in the studies of SiC nanosheets and nanoribbons. It is found that SiC nanosheets and armchair SiC nanoribbons (A-SiCNRs) behave like non-magnetic (NM) wide band gap semiconductors,[13-15] whereas zigzag SiC nanoribbons (Z-SiCNRs) are magnetic[15-16] and exhibit metallic or half-metallic character under narrow width.[15] Furthermore, the magnetic and electronic properties of Z-SiCNRs can be tuned by atomic vacancy[17] or edge reconstruction.[18]

Motivated by the questions as to what are the electronic transport properties of the Z-SiCNR and whether it can be applied as a highly-efficient spintronic device, we conduct theoretical studies on the spin-dependent electronic transport through a SiC nanoribbons with eight zigzag chains (labeled as 8-Z-SiCNR) by using non-equilibrium Green's function in the framework of density functional theory. It is shown that the spin-dependent currents of the ferromagnetic (FM) state presents the pronounced spin filtering and current-limited effects, and the spin polarization (SP) can reach up to about 50% under finite applied biases. On the contrary, obvious oscillation of the spin-polarized currents and polarizations emerge in the antiferromagnetic (AFM) state, and the SP can be as high as 100% under a certain applied bias. The corresponding mechanisms of spin filtering, current-limited as well as spin oscillation effects are subsequently analyzed.

Models and method

The structural model of the SiCNR with eight zigzag chains, which is saturated with one hydrogen atom at each edge Si and C atoms, is shown in Fig. 1(a). The electronic structure and spin-dependent electronic transport properties are studied by using the technique combing the spin density functional theory with nonequilibrium Green's function,[19,20] as implemented in the Atomistix Toolkit code package (ATK).[21,22] The core electrons are described by the Troullier-Martins norm-conserving pseudopotentials, while the valence states of electrons are expanded using linear combinations of atom orbitals (LCAO). The local spin density approximation (LSDA) is used as the exchange-correlation functional. It should be noted that the convergence of LDA is faster and computationally less expensive as compared to that of generalized gradient approximation (GGA) exchange-correlation functional delivering similar results.[10,16,18] The wave functions of all atoms are expanded using double-ζ plus polarization (DZP) basis set.

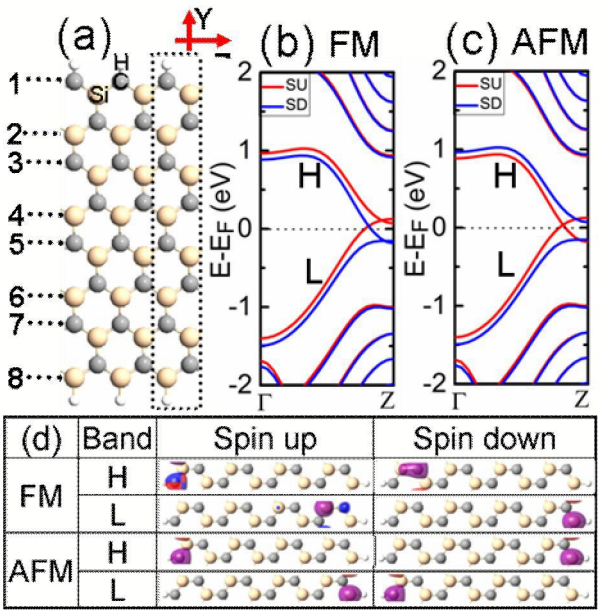

Fig. 1 The geometric and electronic structures of 8-Z-SiCNR. (a) The geometric structure of 8-Z-SiCNR. (b) and (c) Spin-dependent band structures for the FM and AFM states, respectively. SU/SD refers to the spin up/down state. (d) The spin Bloch functions of 8-Z-SiCNR at Z (0, 0, 1/2) point for these H and L bands of the FM and AFM states. The isovalue is set to 0.2.

The Hamiltonian and electronic densities are evaluated in a real space grid with a plan wave cutoff of 150 Ry. A k-point mesh 1×1×100 is adopted to sample the Brillouin zone of the left/right electrodes in the X,Y and Z axis, respectively, where the Z axis denotes the electron transport direction. The geometric structures are relaxed until the force on each atom is less than 0.01 eV/A.

Results and discussion

We first perform total energy calculation for 8-Z-SiCNR considering three spin configurations, i.e., NM, FM and AFM states, respectively. It is found that FM and AFM states are degenerated and have a lower ground state energy as compared to that of NM state, which is consistent with previous results[16] and indicates a spin glass state similar to that of the newly predicted BeS nanoribbons.[23] Thus we choose 8-Z-SiCNR with FM or AFM spin configuration as our system in the following discussion.

The band structures of the FM state is plotted in Fig. 1(b). It is found that there are four bands close to the Fermi Level (E_F) with two bands in each spin up (SU) or down (SD) state crossing each other. We label the band with higher and lower energy as H and L, respectively. The H branch of SU state is completely unoccupied, and L branch is partially occupied. The SD state exhibits reverse behavior. It is also shown that the energy gaps in both spin states are zero, indicating the metallic character of the FM state. The analysis of mulliken population indicates that the magnetic moment per unit cell is about 0.367 μB, smaller than that of the zigzag graphene nanoribbons.[24] Fig. 1(d) depicts the spin-dependent Bloch functions in the Z point. It is clear that the H branch of SU state mainly resides in the C atom in the first zigzag chain, while the Si and C atom in the seventh and eighth chain, respectively, contribute to the L branch of SU state. For the SD state, the Si and C atom in the first and second chain, respectively, contribute to the H branch, while the L branch is localized on the Si atom in the eighth chain.

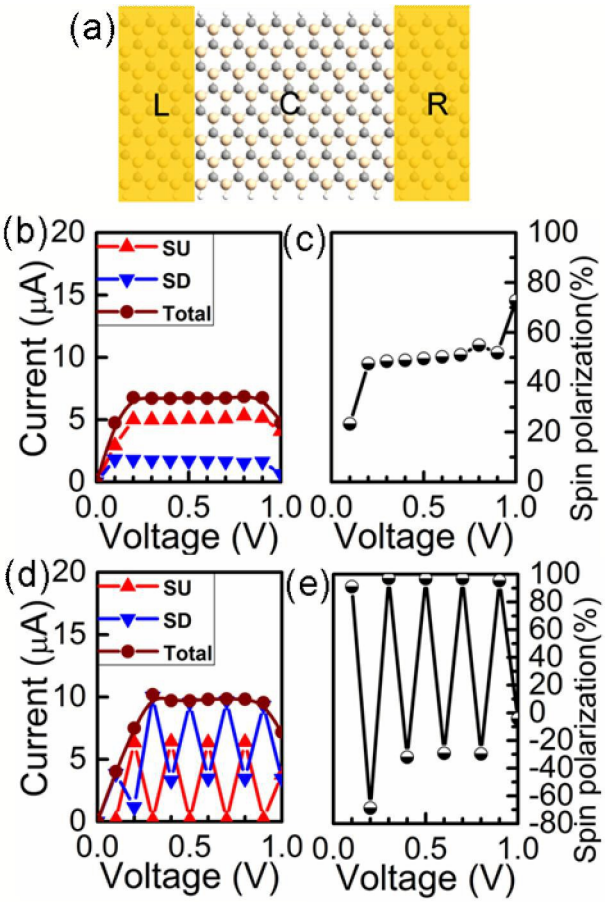

Fig. 2 (a) The two-probe device model for 8-Z-SiCNR. (b)-(e) refer to the *I–V* and spin polarization curves, (b) and (c) for the FM state (d) and (e) for the AFM state, respectively.

For the AFM state, while the two bands close to the EF in the SU state cross with each other, those in the SD state form a direct energy gap at the Z point, as shown in Fig. 1(c). This leads to the partially unoccupied and occupied H and L branches for SU state, respectively, and on the other hand, completely unoccupied and occupied H and L branches for SD state, respectively. As a result, AFM state exhibits half-metallic character with a marginal small magnetic moment 0.002 μB, in accordance with previous report.[15] We also plot the spin-dependent Bloch functions for the AFM state in Fig. 1(d). It can be noted that the H branch of SU(SD) state mainly localized on the C(Si) atom in the first(eighth) chain whereas the L branch of SU(SD) state mostly resides in the Si(C) atom located in the eighth(first) chain.

We then construct a two-probe model (see Fig. 2(a)) to investigate the spin-dependent electronic transport properties of the 8-Z-SiCNR in detail. Such two-probe model consists of left (L) and right (R) electrodes denoted by yellow shadowed areas, between which is the central scattering region (C). Periodic boundary condition in which a supercell with three repeated 8-Z-SiCNR unit cells along the Z direction is applied for each L/R electrode. The key parameter in the study of electronic transport properties of nanodevices is the spin-dependent current, which can be calculated *via* the Landauer-Buttiker formula[25]

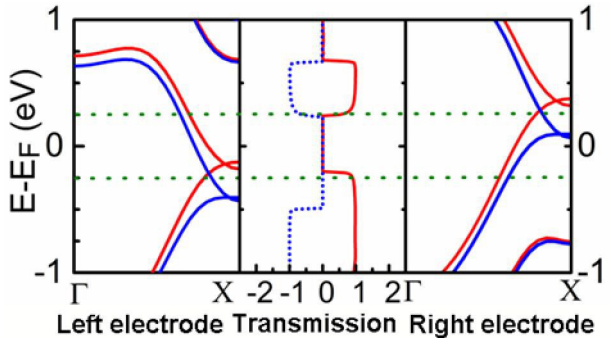

Fig. 3 Band structures for the left electrode, transmission spectra, and band structures for the right electrode under 0.5 V bias. The red lines refer to the spin up state, while the blue lines for the spin down state. The green dotted lines denote the bias window. The upper line refers to the BW_+, while the lower line for the BW_-. The Fermi level is set at zero.

$$I_s(V_b) = \frac{e}{h}\int T_s(E,V_b)\left[f_L(E-\mu_L) - f_R(E-\mu_R)\right]dE, \quad (1)$$

where the s = ↑(spin up) and ↓(spin down), and the total current I_{tot} is the sum of I_s. f_L (f_R) is the Fermi-Dirac distribution function of left(right) electrode with corresponding chemical potential μ_L (μ_R). The electron transmission coefficient $T_s(E, V_b)$ under certain bias V_b is given by

$$T_s(E,V_b) = Tr\left[\Gamma_L G^R \Gamma_R G^A\right]_s, \quad (2)$$

where $G^{R(A)}$ is the retarded (advanced) Green's function of the scattering region and is the contact broadening functions associated with the self-energy of left(right) electrode. It is noted that the integral region in Eq. 1 corresponds to the bias window (BW) from $-eV_b/2$(BW_-) to $+eV_b/2$(BW_+).

Fig. 2(b) depicts the spin dependent as well as total current-voltage (I–V) curves of the FM state. It can be noted that the current of spin up state is much larger than that of spin down state, and SP ($=(I_\uparrow - I_\downarrow)/(I_\uparrow + I_\downarrow)$) can reach as high as 50% under finite biases as shown in Fig. 2(c). Such high SP, larger than the value of 44% in the $Pt/CoFe_2O_4/MgO/Co$ spin filtering device under low temperature,[26] may thus have potential applications in spin filters or spin valves. For further insight into the spin filtering effect of the FM state, we have calculated transmission spectra as well as band structures of the left and right electrodes under 0.5 V bias as plotted in Fig. 3. Overall, the band-structures of left and right electrodes are found to be downward and upward shifted from that without bias, respectively. For spin up state, the L(H) bands of the left and right electrodes start to overlap with each other at the energy close to the BW_- (BW_+), which facilitates the transmission of electron, leading consequently to relatively larger current in the device. However, the spin down electrons can not easily propagate through the nanoribbon at the energy close to BW_-, which can be attributed to the fact that there is no overlap between L bands of the left and right electrodes near BW_-. As a result, smaller current is expected for the spin down state, inducing spin polarization of current.

We also note that the spin up (down) as well as total currents display pronounced current-limited effects with saturated values of

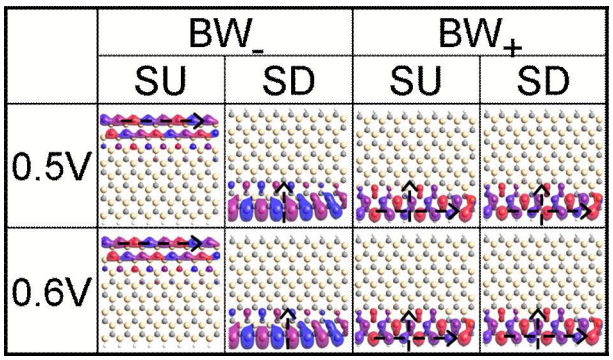

Fig. 4 The transmission eigenstates of the central scattering region for the FM state at the BW_- and BW_+ under the biases of 0.5 and 0.6 V, respectively. The isovalue is set to 0.15.

5.1 μA (1.7 μA) and 6.8 μA for spin up (down) and total currents respectively. It is found that, with the increase of bias voltages, the degree of overlaps between the H (L) bands of the left and right electrodes and the transmission gap near the Fermi level gradually decreases and increases, respectively, while the areas of the transmission spectra inside the bias window are almost the same (see Supporting information Figure S1). Consequently, the spin up (down) current is expected to keep constant with the increase of bias voltages.

In order to elucidate the electron transmission picture intuitively, we plot the transmission eigenstates of the central scattering region at the energy BW_- (BW_+) with the applied bias voltages of 0.5 and 0.6 V, respectively, as depicted in Fig. 4. Firstly, we note that, for both bias voltages of 0.5 and 0.6 V, the transmission eigenstates for spin up and down states exhibit same profiles, which is consistent with the current limited effect shown in Fig. 2(b). Secondly, at the energy of BW_-, the spin up eigenstate resides almost in the first zigzag chain, while it is mainly localized on the Si atoms of the seventh and eighth chains for spin down eigenstate. It can be also noted that the distribution patterns are along and perpendicular to the electron transport direction for spin up and down states, respectively. For the case of BW_+, both the spin up and down states are mainly composed of mixtures of the p_x orbitals of Si atoms in the seventh chain and Si and C atoms in the eighth chain, which can be decomposed into two parts that are parallel and perpendicular to the electron transport direction.

For the AFM state, quite interestingly, it is found that the spin up (down) currents as well as SP exhibit abnormal oscillation with applied bias voltages as shown in Fig. 2(d) and (e). At biases of 0.3, 0.5, and 0.7 V, the value of currents are found to be almost zero for spin up state and 9.76 μA for spin down state, while they are 6.37 μA and 3.41 μA at biases of 0.4, 0.6, and 0.8 V, thereby leading to the oscillation pattern of currents. Correspondingly, the SP also exhibits oscillation behaviors with values as high as 100% at certain bias voltages, reflecting a perfect spin filtering performance. Similar to the case of FM state, the total currents also display pronounced current-limited effect with a larger saturated value of current.

In order to understand the oscillation patterns of the spin-polarized currents, we show the transmission spectra and band structures of the left and right electrodes at the bias voltages of 0.5 and 0.6 V in Fig. 5. It can be found that, the spin up H and L bands of the left electrode cross each other near the energy of BW_-, leading to that the electrons can not propagate through the nanoribbon due to

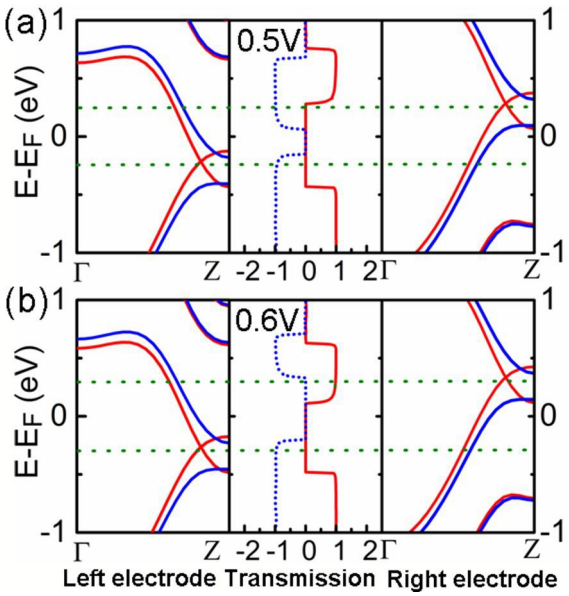

Fig. 5 Band structures for the left electrode, transmission spectra, and band structures for the right electrode under the biases of 0.5 and 0.6 V, respectively. The red lines refer to the spin up state, while the blue lines for the spin down state.

the competition between the both edges. While, the spin down electrons from the L band of the right electrode can always transmit to the left electrode, and the transmission probability is close to 1. Another, the spin up H and L bands always cross each other near the BW_+, and may impact on the spin down L band of the right electrode. It would make the spin up and down electrons interfere with each other, resulting in the alternate transmission of the spin up and down electrons with the biases increasing (see Supporting Information Figure S2).

To more intuitively understand the spin oscillation behaviors for the AFM state, as shown in Fig. 6, we gives the transmission eigenstates of the AFM state at the BW_- and BW_+ under the biases of 0.4, 0.5, 0.6, and 0.7 V, respectively. Clearly, at the 0.4 and 0.6 V biases, the spin up eigenstates are mainly localized on the Si atoms of the eighth and seventh chains at the energy of BW_-, which are perpendicular to the transport direction and give no contributions to the current. On the contrary, the spin down eigenstates are mainly distributed on the first zigzag chain, and are parallel to the transport direction, then to be effective for the spin down electrons propagating through. For another, at the energy of BW_+, the spin up eigenstates are a mixture of the p_x orbitals of the Si and C atoms in the eighth chain and the Si atom in the seventh chain. Only the decomposed parallel direction contributes to the current, but the perpendicular one not. While, the spin down states are completely empty and give no any contribution to the currents. Differently, for the case of 0.5 and 0.7 V, the spin up eigenstates at the BW_- are completely empty, and the spin down ones are the same to that of 0.4 and 0.6 V. The spin up eigenstates at the BW_+ are mainly localized on the Si atoms of the eighth and seventh chains, but perpendicular to the transport direction and giving no contributions to the current. The spin down ones are a mixture of the p_x orbitals of the Si and C atoms in the eighth chain and the Si atom in the seventh chain. Only the decomposed parallel direction contributes to the current, but the perpendicular direction not.

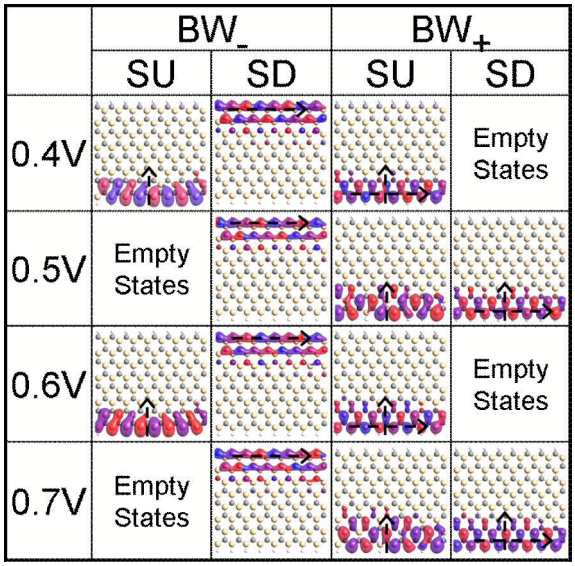

Fig. 6 The transmission eigenstates of the central scattering region for the AFM state at the BW_- and BW_+ under the biases of 0.4, 0.5, 0.6, and 0.7 V, respectively. The isovalue is set to 0.15.

In order to lend more support towards the intuitive pictures described in the previous section, we have further ventured to analyze the transmission pathways, also called local currents,[27] in the central scattering region of the 8-Z-SiCNR nanodevice. The transmission pathways is an analysis option which splits the transmission coefficient into local bond contributions, T_{ij}. The pathways have the property that if the system is divided into two parts (A, B), then the pathways across the boundary between A and B sum up to the total transmission coefficient

$$T(E)=\sum_{i\in A,\, j\in B} T_{ij}(E)\cdot \qquad (3)$$

The transmission pathways at the energy of BW_- and BW_+ calculated with this method are found to be same for both FM and AFM states as shown in Fig. 7. At the energy of BW–, it is shown that the electron currents flow mainly along the first chain and the local currents are of type of bond current, i.e, *via* C→Si→C chemical bonds. The main contributions to local currents are from spin up (down) electrons for FM (AFM) state. For the case of BW+, the local currents are mainly composed of three pathways with one bond type *via* the Si→C→Si chemical bonds in the eighth chain and another two hopping type *via* Si→Si hopping in the eighth chain and Si→Si→Si hopping between the seventh and eighth chains.

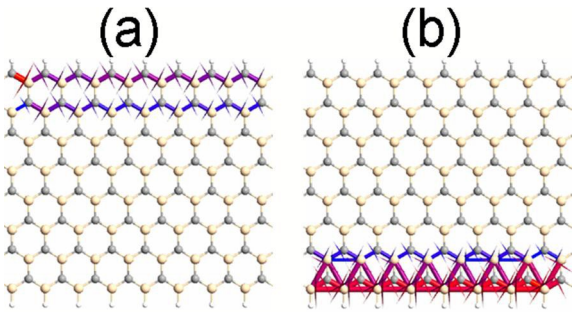

Fig. 7 The transmission pathways at the BW_- (a) and BW_+ (b).

Conclusions

In summary, we have carried out theoretical and computational investigation on the spin-dependent electronic transport properties of the zigzag SiC nanoribbon, which exhibits promising applications in spintronic nanodevices. Our results demonstrate that the FM state of the 8-Z-SiCNR is of metallic character, and its spin-polarized *I–V* curves display spin filtering and current-limited effects. On the other hand, the AFM state with half-metallic character presents abnormal spin-dependent current oscillation behaviors. Through detailed analysis of electronic band structures of the left/right electrode as well as the transmission eigenstates of the central scattering regime, we are then able to understand the exotic *I–V* behaviors of the FM and AFM state. The band structures analysis of left/right electrode for FM state show that the spin up bands of the two electrode can overlap with each other near the BW_, whereas there is nearly no overlap between spin down bands of the left and right electrode, which leads to obvious spin-polarized current. For AFM state, the abnormal spin-dependent current oscillation may be attributed to fact that the spin up H and L bands and spin down H band of the right electrode interfere with each other, resulting in the alternate transmission of the spin up and down electrons with the change of the applied biases. Tracing the origins of the exotic electronic transport properties of zigzag SiC nanoribbon, our work is hoped to provide some design principles for the preparations and applications of future spin nanodevices.

Acknowledgements

This work was supported by the National Natural Science Foundation of China (Grant Nos. 11304084, U1304109, U1304518, and 11247012), the Natural Science Foundation of Henan Province (Grant Nos. 122300413208 and 152300410085), and the High Performance Computing Centre of Henan Normal University.

Notes and references

[a]*College of Physics and Electronic engineering, Henan Normal University, Xinxiang 453007, China.*
E-mail address: ypan@htu.edu.cn; xiacongxin@htu.edu.cn; Fax: +86 373 3329346.
[b]*Division of Materials Science, Nanyang Technological University, 50 Nanyang Avenue, Singapore 639798, Singapore.*
[c]*Beijing National Laboratory for Condensed Matter Physics, Institute of Physics, Chinese Academy of Sciences, Beijing 100190, China.*

1 S. A. Wolf, D. D. Awschalom, R. A. Buhrman, J. M. Daughton, S. von Molnár, M. L. Roukes,A. Y. Chtchelkanova and D. M. Treger, *Science*, 2001, **294**, 1488−1495.
2 K. S. Novoselov, A. K. Geim, S. V. Morozov, D. Jiang, Y. Zhang and S. V. Dubonos. *Science*, 2004, **306**, 666–669.
3 L. Wang, X. Chen, Y. Hu, A. Yu and W. Lu, *Nanoscale*, 2014, **6**, 12769−12779.
4 S. Vaziri, G. Lupina, C. Henkel, A. D. Smith, M. Östling, J. Dabrowski, G. Lippert, W. Mehr and M. C. Lemme, *Nano Lett.*, 2013, **13**, 1435−1439.
5 E. U. Stützel, M. Burghard, K. Kern, F. Traversi, F. Nichele, R. Sordan, *Small*, 2010, **6**, 2822−2825.
6 X. Q. Deng, Z. H. Zhang, G. P. Tang, Z. Q. Fan and C. H. Yang, *Carbon*, 2014, **66**, 646−653.
7 J. Guo, D. Gunlycke and C. T. White, *Appl. Phys. Lett.*, 2008, **92**, 163109.
8 W. Y. Kim and K. S. Kim, *Nature Nanotech.*, 2008, **3**, 408−412.
9 S. M. M. Dubois, X. Declerck, J. C. Charlier and M. C. Payne, *ACS Nano*, 2013,**7**, 4578−4585.
10 Y. An, K. Wang, G. Jia, T. Wang, Z. Jiao, Z. Fu, X. Chu, G. Xu and C. Yang, *RSC Adv.*, 2014, **4**, 46934−46939.
11 H. Zeng, C. Zhi, Z. Zhang, X. Wei, X. Wang, W. Guo, Y. Bando and D. Golberg, *Nano Lett.*, 2010, **10**, 5049−5055.
12 X. H. Sun, C. P. Li, W. K. Wong, N. B. Wong, C. S. Lee, S. T. Lee, B. K. Teo, *J. Am. Chem. Soc.*, 2002, **124**, 14464–14471.
13 H. Sahin, S. Cahangirov, M. Topsakal, E. Bekaroglu, Akturk, R. T. Senger and S. Ciraci, *Phys. Rev. B*, 2009, **80** 155453.
14 E. Bekaroglu, M. Topsakal, S. Cahangirov and S. Ciraci, *Phys. Rev. B*, 2010, **81**, 075433.
15 L. Sun, Y. Li, Z. Li, Q. Li, Z. Zhou, Z. Chen, J. Yang and J. G. Hou, *J. Chem. Phys.*, 2008, **129**, 174114.
16 P. Lou and J. Y. Lee, *J. Phys. Chem. C*, 2009, **113**, 12637−12640.
17 J. M. Morbec and G. Rahman, *Phys. Rev. B*, 2013, **87**, 115428.
18 A. Lopez-Bezanilla, J. Huang, P. R. C. Kent and B. G. Sumpter, *J. Phys. Chem. C*, 2013, **117**, 15447−15455.
19 M. Brandbyge, J. L. Mozos, P. Ordejón, J. Taylor and K. Stokbro, *Phys. Rev. B*, 2002, **65**, 165401.
20 J. M. Soler, E. Artacho, J. D. Gale, A. García, J. Junquera, P. Ordejón and D. Sánchez-Portal, *J. Phys.: Condens. Matter* 2002, **14**, 2745−2779.
21 Atomistix ToolKit, 2014.03, see http://quantumwise.com/.
22 J. Taylor, H. Guo and J. Wang, *Phys. Rev. B*, 2001, **63**, 121104.
23 J. Yu and W. Guo, *J. Phys. Chem. Lett.*, 2013, **4**, 1856−1860
24 L. Pisani, J. A. Chan, B. Montanari and N. M. Harrison, *Phys. Rev. B*, 2007, **75**, 064418.
25 M. Büttiker, Y. Imry, R. Landauer and S. Pinhas, *Phys. Rev. B*, 1985, **31**, 6207−6215.
26 Y. K. Takahashi, S. Kasai, T. Furubaysashi, S. Mitani, K. Inomata and K. Hono, *Appl. Phys. Lett.*, 2010, **96**, 072512.
27 G. C. Solomon, C. Herrmann, T. Hansen, V. Mujica, M. A. Ratner, *Nat. Chem.*, 2010, **2**, 223−228.

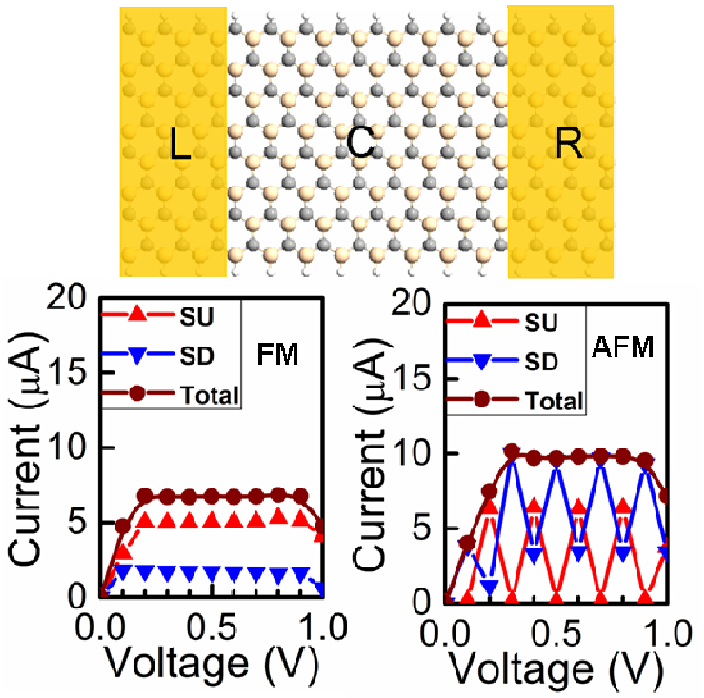

The zigzag SiC nanoribbon devices exhibits a variety of exotic physical properties such as spin filtering, current-limited, and oscillation effects.